

Intention-Aware Control Based on Belief-Space Specifications and Stochastic Expansion

Zengjie Zhang¹, Zhiyong Sun¹, and Sofie Haesaert¹

Abstract—This paper develops a correct-by-design controller for an autonomous vehicle interacting with opponent vehicles with unknown intentions. We define an intention-aware control problem incorporating epistemic uncertainties of the opponent vehicles and model their intentions as discrete-valued random variables. Then, we focus on a control objective specified as belief-space temporal logic specifications. From this stochastic control problem, we derive a sound deterministic control problem using stochastic expansion and solve it using shrinking-horizon model predictive control. The solved intention-aware controller allows a vehicle to adjust its behaviors according to its opponents' intentions. It ensures provable safety by restricting the probabilistic risk under a desired level. We show with experimental studies that the proposed method ensures strict limitation of risk probabilities, validating its efficacy in autonomous driving cases. This work provides a novel solution for the risk-aware control of interactive vehicles with formal safety guarantees.

I. INTRODUCTION

When an autonomous vehicle interacts with other traffic participants, the awareness of the intentions of these participants strongly impacts the safety and reliability of its decision-making. This has motivated the studies on *intention-aware* motion planning [1]–[3]. Fig. 1 shows an intersection case where an ego vehicle (EV) plans a left turn while avoiding collisions with opponent vehicles (OVs) and pedestrians from the opposite direction. Understanding the intentions of these participants (e.g., moving fast or slowly) facilitates the design of a safe and flexible policy. Intention-aware motion planning has been formulated as a partially observable Markov decision process (POMDP) [4], where intentions are discrete-valued unobservable variables encoding uncertain policies [5]. Decision-making with the awareness of intentions aims at a safe policy for all assumed opponents' behaviors, rendering a challenging planning problem with complex uncertainties, for which planning-based methods, such as reinforcement learning, have been used [6]. However, these methods rely on precise agent models, causing *sim-to-real* issues when models are imprecise [7]. Moreover, these solutions hardly ensure formal safety guarantees or probable risk restrictions [8]. These concerns enforce the need for an intention-aware controller that is correct by design and is robust to modeling errors, which has not been addressed in the literature.

*This work was supported by the European project SymAware under grant No. 101070802.

¹Zengjie Zhang, Zhiyong Sun, and Sofie Haesaert are with the Department of Electrical Engineering, Eindhoven University of Technology, PO Box 513, 5600 MB Eindhoven, Netherlands {z.zhang3, z.sun, s.haesaert}@tue.nl

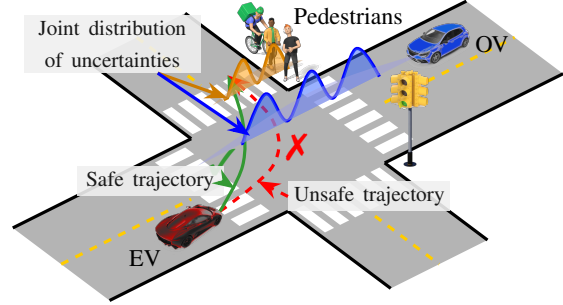


Fig. 1: An intersection case where an EV plans a collision-free left turn, aiming at a safe trajectory for the complex modeling-intention uncertainties of the OV and pedestrians. Understanding the intentions of the OV and the pedestrians helps the EV make safe decisions.

Control of autonomous agents with stochastic uncertainties has been formulated as a stochastic control problem subject to probability constraints [9]. Beyond this, formal safety guarantees have been specified as temporal logic formulas, such as Signal Temporal Logic (STL) [10] and Linear-time Temporal Logic (LTL) [11], aiming at a *risk-aware* controller that restricts risk probabilities to certain levels [12]. A stochastic control problem with formal specifications can be solved using Model Predictive Control (MPC) [13] and abstraction-based methods [14]. Belief-space specifications, such as Partially observable computation tree logic (POCTL) [15], Distribution Temporal Logic (DTL) [16], Gaussian DTL [17], and probabilistic STL [18] have been proposed to convert a stochastic control problem into a more tractable deterministic belief-space control problem [19]. Specification decomposition [20] and splitting [21] approaches improve the efficiency of solving a control problem with STL.

However, these existing control methods mainly apply to uncertainties with Gaussian or bounded-support distributions [22]. As to be addressed later, intention-aware control requires characterizing complex uncertainties with non-Gaussian or multi-modal distributions, thus remaining an open and challenging problem. An effective approach to precisely characterize nontrivial probabilistic distributions is stochastic expansion [23]. As a representative method of stochastic expansion, Polynomial Chaos Expansion (PCE) can efficiently characterize an arbitrary probabilistic model by decomposing it to a linear combination of a finite number of orthogonal bases. It has shown advantages in robust

A. Modeling Traffic Participants

We consider a general traffic system containing a deterministic EV and multiple uncertain opponent participants. Without losing generality, we assume all opponent participants are vehicles (OVs). The EV is described as the following deterministic discrete-time dynamic model [29],

$$\text{EV} : \begin{cases} x_{k+1} = Ax_k + Bu_k + d_k, \\ y_k = Cx_k, \end{cases} \quad (1)$$

where $x_k \in \mathbb{R}^n$, $u_k \in \mathbb{R}^m$, $d_k \in \mathbb{R}^d$, and $y_k \in \mathbb{R}^l$ are the state, the control input, the external input, and the measurement output of the EV, respectively, at time $k \in \mathbb{N}$, and $A \in \mathbb{R}^{n \times n}$, $B \in \mathbb{R}^{n \times m}$, $C \in \mathbb{R}^{l \times n}$ are constant matrices, where $n, m, l \in \mathbb{Z}^+$. Additionally, d_k for $k \in \mathbb{N}$ is a bounded external input denoting the deterministic disturbance or modeling errors of the EV. A deterministic model for EV similar to Eq. (1) is common in practice [29]. A nonlinear vehicle model like a bicycle model in [30] can be represented as Eq. (1) after linearization, as addressed in Appx.-B.

Each OV has a stochastic linear dynamic model [31],

$$\text{OV} : \begin{cases} z_{k+1} = F(\theta)z_k + G(\theta)v_k, \\ w_k = H(\theta)z_k, \end{cases} \quad (2)$$

where z_k , v_k , and w_k are state, control input, and output of the OV with certain dimensions, $F(\theta)$, $G(\theta)$, and $H(\theta)$ are parametric matrices dependent on a random parameter θ subject to a multi-dimensional joint probabilistic density function (PDF) p_θ . All vectors and matrices are of proper dimensions. We assume the elements of θ are independent and identically distributed (i.i.d) random variables with finite second-order moments. Such models with parametric uncertainties have been commonly used [31]. Here, Eq. (2) allows a heterogeneous setting, where the OVs may be of different dimensions and parametric matrices. A nonlinear bicycle model can be represented using the general uncertain model in Eq. (2) after linearization, as addressed in Appx.-C. In this paper, we also use an OV model defined in (2) to represent the behavior of a group of pedestrians [32].

The overall model of all opponent traffic participants can be represented as the following compact form,

$$\text{OVs} : \begin{cases} \bar{z}_{k+1} = \mathbf{F}(\bar{\theta})\bar{z}_k + \mathbf{G}(\bar{\theta})\bar{v}_k, \\ \bar{w}_k = \mathbf{H}(\bar{\theta})\bar{z}_k, \end{cases} \quad (3)$$

where $\bar{z}_k \in \mathbb{R}^p$, $\bar{v}_k \in \mathbb{R}^q$, $\bar{w}_k \in \mathbb{R}^r$, and $\bar{\theta} \in \mathbb{R}^t$ are vectors with the joint state, input, output, and uncertain parameters of all OVs, respectively, and $\mathbf{F} \in \mathbb{R}^{p \times p}$, $\mathbf{G} \in \mathbb{R}^{p \times q}$, and $\mathbf{H} \in \mathbb{R}^{r \times p}$ are augmented matrices containing the parametric matrices of the OVs, with $p, q, r, t \in \mathbb{Z}^+$ being proper dimensions.

B. Random Intentions with Epistemic Uncertainty

For each OV, we define a discrete-valued intention variable ι sampled from a finite intent set I with a probabilistic distribution p_ι . Based on this, we assume that each OV is controlled by the following intention-encoded policy,

$$v_k := K(\iota)\bar{w}_k + L(\iota)\tau_k, \quad (4)$$

where τ_k is a predefined feedforward control input for $k \in \mathbb{N}$ with proper dimensions, and $K(\iota)$ and $L(\iota)$ are the feedback and the feedforward control gain matrices of proper dimensions, respectively. Eq. (4) defines a representative control policy that covers feedback control, feedforward control, and interaction with other OVs. Substituting Eq. (4) to Eq. (2), we obtain the closed-loop dynamic model of OV as

$$z_{k+1} = F(\bar{\theta})z_k + G(\bar{\theta})K(\bar{\iota})\mathbf{H}(\bar{\theta})\bar{z}_k + G(\bar{\theta})L(\bar{\iota})\tau_k, \quad (5)$$

where $\bar{\iota}$ is the joint intention of all OVs. Eq. 5 then can be compactly written as

$$\text{OVs(closed loop)} : \begin{cases} \bar{z}_{k+1} = \bar{\mathbf{F}}(\eta)\bar{z}_k + \bar{\mathbf{G}}(\eta)\bar{\tau}_k, \\ \bar{w}_k = \mathbf{H}(\eta)\bar{z}_k, \end{cases} \quad (6)$$

where $\bar{\tau}_k$ is the vector of the joint feedforward control inputs of the OVs, $\bar{\mathbf{F}}$ and $\bar{\mathbf{G}}$ are joint matrices derived from Eq. (5), and $\eta := [\bar{\theta}^\top \bar{\iota}^\top]^\top$ is a joint random variable containing the uncertain parameters $\bar{\theta}$ and joint intentions $\bar{\iota}$ of the OVs. Due to the continuous nature of $\bar{\theta}$ and the discrete nature of $\bar{\iota}$, the random variable η is usually subject to a complex distribution.

With an arbitrary initial condition $x_0 \in \mathbb{R}^n$, the EV model in (1) generates a deterministic output trajectory $\mathbf{y} := y_0 y_1 y_2 \dots$. In the meantime, with the influence of the random variable η , the OV model in (6) generates a stochastic output trajectory $\mathbf{w} := \bar{w}_0 \bar{w}_1 \bar{w}_2 \dots$. Due to the complex distribution of η , the trajectories \mathbf{w} may follow a complex multimodal joint distribution, as illustrated in Fig. 1. Quantifying such complex uncertainty poses a challenge to solving the intention-aware control problem. Fortunately, such uncertainty has an *epistemic* nature since the distribution of η is time-invariant and can be learned with sufficient data [25]. On the contrary is *aleatory* uncertainty that can never be precisely characterized by a time-invariant probabilistic distribution, such as random noise [33]. Epistemic uncertainty can be precisely and tractably characterized using stochastic expansion methods like PCE [23]. In this sense, PCE shows great potential in solving the intention-aware control problem that requires precise quantification of epistemic uncertainty.

C. Describing Tasks Using Belief-Space Specifications

Practical driving tasks can be represented as physical constraints. For vehicle models defined in Sec. III-A, a typical constraint has the following probabilistic form [9],

$$P(\gamma^\top \bar{w}_k \leq \beta - \alpha^\top y_k) \geq 1 - \varepsilon, \quad k \in \mathbb{N}, \quad (7)$$

where $y_k \in \mathbb{R}^l$, $\bar{w}_k \in \mathbb{R}^r$ are outputs of the EV and the OVs given by Eq. (1) and Eq. (6), respectively, α , β , γ are constant coefficients with proper dimensions, and $\varepsilon \in [0, 1]$ is a risk restriction scalar. The constraint Eq. (8) implies a quantified risk restriction. If \bar{w}_k is Gaussian for all $k \in \mathbb{N}$, according to [34], the probabilistic constraint Eq. (7) is equivalent to

$$\alpha^\top y_k + \gamma^\top \mu_{\bar{w}_k} + \kappa_\varepsilon \sqrt{\gamma^\top \Sigma_{\bar{w}_k} \gamma} - \beta \leq 0, \quad (8)$$

where $\mu_{\bar{w}_k} \in \mathbb{R}^r$ and $\Sigma_{\bar{w}_k} \in \mathbb{R}^{r \times r}$ are the expected value and the covariance of \bar{w}_k , respectively, and $\kappa_\varepsilon = \Psi^{-1}(1 - \varepsilon)$ is a scalar

with Ψ being the cumulative probability function of the normal distribution. However, the equivalence between Eq. (7) and Eq. (8) does not hold if \bar{w}_k is non-Gaussian, for which conservativeness is inevitably introduced. Consider that \bar{w}_k has finite statistic moments of all orders. Let $\mathcal{D}(\mu_{\bar{w}_k}, \Sigma_{\bar{w}_k})$ be the set of all random variables that have the same expected value and covariance as \bar{w}_k . Then, the following constraint,

$$\inf_{\omega \in \mathcal{D}(\mu_{\bar{w}_k}, \Sigma_{\bar{w}_k})} P(\gamma^\top \omega \leq \beta - \alpha^\top y_k) \geq 1 - \varepsilon, \quad k \in \mathbb{N}, \quad (9)$$

is equivalent to Eq. (8) but with $\kappa_\varepsilon = \sqrt{(1-\varepsilon)/\varepsilon}$ [34]. Note that Eq. (9) is conservative to Eq. (7) due to the \inf operator. Let $\mathcal{B}^r := \mathbb{R}^r \times \mathbf{S}^r$ be a belief space of r -dimensional random variables that have known first- and second-order moments, where $\mathbf{S}^r \subset \mathbb{R}^{r \times r}$ is the set of all positive semi-definite matrices, such that $(\mu_{\bar{w}_k}, \Sigma_{\bar{w}_k}) \in \mathcal{B}^r$, $\forall k \in \mathbb{N}$. Then, Eq. (8) serves as an inequality constraint defined on the belief space \mathcal{B}^r . In this way, we build a connection between probabilistic constraints and belief-space inequalities, that is, any probabilistic constraint in the form of Eq. (7) corresponds to a sound belief-space inequality as Eq. (8).

Now, we extend the belief-space inequalities as Eq. (8) into belief-space formal specifications as follows.

Definition 1 (Distribution Signal Temporal Logic (DSTL)): For random signals $\mathbf{y} := y_0 y_1 \dots$ generated by Eq. (1) and $\mathbf{w} := \bar{w}_0 \bar{w}_1 \dots$ generated by Eq. (6), a DSTL formula φ defined over the joint signal $(\mathbf{y}, \mathbf{w}) := (y_0, \bar{w}_0)(y_1, \bar{w}_1) \dots$ has the following inductively defined syntax,

$$\varphi := \top \mid (\vee, \varepsilon) \mid \neg \varphi \mid \varphi_1 \wedge \varphi_2 \mid \varphi_1 \mathbf{U}_{[a,b]} \varphi_2,$$

where φ , φ_1 and φ_2 are DSTL formulas, (\vee, ε) is a belief-space predicate associated with a mapping $g_\varepsilon : \mathbb{R}^l \times \mathcal{B}^r \rightarrow \mathbb{R}$ via $(\vee, \varepsilon) := \begin{cases} \top, & g_\varepsilon(y_k, (\mu_{\bar{w}_k}, \Sigma_{\bar{w}_k})) \leq 0 \\ \neg \top, & g_\varepsilon(y_k, (\mu_{\bar{w}_k}, \Sigma_{\bar{w}_k})) > 0 \end{cases}$, for a given time $k \in \mathbb{N}$, where g_ε is defined as the left hand of the inequality Eq. (8), and $\mathbf{U}_{[a,b]}$ is the *until* operator bounded with time interval $[a, b]$, where $a, b \in \mathbb{N}$ and $a \leq b$. We define the *disjunction*, *eventually*, and *always* operators as $\varphi_1 \vee \varphi_2 := \neg(\neg \varphi_1 \wedge \neg \varphi_2)$, $\mathbf{F}_{[a,b]} \varphi := \top \mathbf{U}_{[a,b]} \varphi$, $\mathbf{G}_{[a,b]} \varphi := \neg(\top \mathbf{U}_{[a,b]} \neg \varphi)$. The semantics of the DSTL $((\mathbf{y}, \mathbf{w}), k) \models \varphi$ are recursively defined as follows,

$$\begin{aligned} ((\mathbf{y}, \mathbf{w}), k) &\models (\vee, \varepsilon) \leftrightarrow g_\varepsilon(y_k, (\mu_{\bar{w}_k}, \Sigma_{\bar{w}_k})) \leq 0, \\ ((\mathbf{y}, \mathbf{w}), k) &\models \neg \varphi \leftrightarrow \neg((\mathbf{y}, \mathbf{w}), k) \models \varphi, \\ ((\mathbf{y}, \mathbf{w}), k) &\models \varphi_1 \wedge \varphi_2 \leftrightarrow ((\mathbf{y}, \mathbf{w}), k) \models \varphi_1 \wedge ((\mathbf{y}, \mathbf{w}), k) \models \varphi_2, \\ ((\mathbf{y}, \mathbf{w}), k) &\models \varphi_1 \vee \varphi_2 \leftrightarrow ((\mathbf{y}, \mathbf{w}), k) \models \varphi_1 \vee ((\mathbf{y}, \mathbf{w}), k) \models \varphi_2, \\ ((\mathbf{y}, \mathbf{w}), k) &\models \mathbf{F}_{[a,b]} \varphi \leftrightarrow \exists k' \in [k+a, k+b], ((\mathbf{y}, \mathbf{w}), k') \models \varphi, \\ ((\mathbf{y}, \mathbf{w}), k) &\models \mathbf{G}_{[a,b]} \varphi \leftrightarrow \forall k' \in [k+a, k+b], ((\mathbf{y}, \mathbf{w}), k') \models \varphi, \\ ((\mathbf{y}, \mathbf{w}), k) &\models \varphi_1 \mathbf{U}_{[a,b]} \varphi_2 \leftrightarrow \exists k' \in [k+a, k+b], \\ &\text{s.t. } ((\mathbf{y}, \mathbf{w}), k') \models \varphi_2, \text{ and } \forall k'' \in [k, k'], ((\mathbf{y}, \mathbf{w}), k'') \models \varphi_1. \end{aligned}$$

For $k=0$, the symbol k is omitted, rendering $(\mathbf{y}, \mathbf{w}) \models \varphi$. \square

Each DSTL predicate renders a belief-space inequality equivalent to a sound probabilistic constraint like Eq. (9), building a connection between DSTL and probabilistic constraints. DSTL can be recognized as a generalization of STL (See Appx.-A) to belief spaces or an extension of DTL [16] or Gaussian DTL [17] to real-valued signals.

IV. TRACTABLE CONTROL SOLUTION BASED ON PCE

With the mathematical models defined in Sec. III, Problem 1 can be reformulated as the following formal control problem specified by a DSTL formula and solved using the following *shrinking-horizon* MPC-based approach [13] within a predefined control horizon $\mathcal{H} := \{0, 1, \dots, N-1\}$, $N \in \mathbb{Z}^+$.

Problem 2 (Formal Intention-Aware Control):

For the mathematic models defined in Sec. III, solve a history- and intention-dependent controller $\pi : \mathbf{Y}^+ \times \mathcal{P} \rightarrow \mathbf{U}$ for the EV, where \mathbf{Y}^+ is the set of all output trajectories of the EV, \mathcal{P} is the space of all possible distributions of the intentions of the OVs, and \mathbf{U} is the feasible control set of the EV, such that the output trajectories \mathbf{y} and \mathbf{w} satisfy a predefined DSTL formula, i.e., $(\mathbf{y}, \mathbf{w}) \models \varphi$. \square

Shrinking-Horizon MPC-based Solution: For any time $k \in \mathbb{N}$ with historical measurements $y_0 y_1 \dots y_k \in \mathbf{Y}^+$, solve the following stochastic optimization problem,

$$\min_{\tilde{\mathbf{u}}_k} \sum_{i=0}^{N-k-1} \tilde{\mathbf{u}}_{i|k}^\top R \tilde{\mathbf{u}}_{i|k} \quad (10a)$$

$$\text{s.t. } \tilde{\mathbf{x}}_{i+1|k} = A \tilde{\mathbf{x}}_{i|k} + B \tilde{\mathbf{u}}_{i|k}, \quad (10b)$$

$$\tilde{\mathbf{u}}_{i|k} \in \mathbf{U}, \quad \forall i \in \{0, 1, \dots, N-k-1\}, \quad (10c)$$

$$\tilde{\mathbf{y}}_{i+k|k} = C \tilde{\mathbf{x}}_{i|k}, \quad \forall i \in \{0, 1, \dots, N-k\}, \quad (10d)$$

$$\tilde{\mathbf{y}}_{r|k} = y_r, \quad \forall r \in \{0, 1, \dots, k\}, \quad (10e)$$

$$\tilde{\mathbf{z}}_{i+1} = \mathbf{F}(\eta) \tilde{\mathbf{z}}_i + \mathbf{G}(\eta) \tilde{\mathbf{t}}_i, \quad \forall i \in \mathcal{H}, \quad (10f)$$

$$\tilde{\mathbf{w}}_i = \mathbf{H}(\eta) \tilde{\mathbf{z}}_i, \quad \forall i \in \mathcal{H} \cup \{N\}, \quad (10g)$$

$$(\tilde{\mathbf{y}}_k, \mathbf{w}) \models \varphi, \quad (10h)$$

where $\tilde{\mathbf{x}}_k := \tilde{x}_{0|k} \dots \tilde{x}_{N-k|k}$, $\tilde{\mathbf{u}}_k := \tilde{u}_{0|k} \dots \tilde{u}_{N-k-1|k}$, and $\tilde{\mathbf{y}}_k := \tilde{y}_{0|k} \dots \tilde{y}_{N|k}$ are decision variables for the state, the input, and the output at time k , $R \in \mathbb{R}^{m \times m}$ is a cost matrix, $\mathbf{U} \subseteq \mathbb{R}^m$ is a control constraint set, and $\mathbf{w} := \bar{w}_0 \bar{w}_1 \dots \bar{w}_N$ is the measurement trajectory of the OVs generated by Eq. (2) with an intention-dependent policy in (4). Having solved $\tilde{\mathbf{u}}_k$, apply its first element $\tilde{u}_{0|k}$ to the EV model in Eq. (1) as the control input.

Remark 1 (Robustness): The control scheme above is closed-loop since the control input $\tilde{u}_{0|k}$ at time $k \in \mathbb{N}$ depends on the historical measurements $y_0 y_1 \dots y_k$. Thus, the controller is robust to the unknown disturbance d_k in Eq. (1).

The solution above is challenging to solve due to the complex joint uncertainty brought up by η . Now, we provide an efficient control solution facilitated by PCE. As a typical stochastic expansion approach, PCE allows the stochastic parameters $\tilde{\mathbf{F}}$, $\tilde{\mathbf{G}}$, and $\tilde{\mathbf{H}}$ in Eq. (6) to be approximated as $\tilde{\mathbf{F}} = \sum_{i=0}^{L-1} \hat{\mathbf{F}}_i \Phi_i$, $\tilde{\mathbf{G}} = \sum_{i=0}^{L-1} \hat{\mathbf{G}}_i \Phi_i$, and $\tilde{\mathbf{H}} = \sum_{i=0}^{L-1} \hat{\mathbf{H}}_i \Phi_i$, where $L \in \mathbb{Z}^+$ is a predefined finite expansion order, $\Phi = \{\Phi_0 \Phi_1 \dots \Phi_{L-1}\}$ is a series of orthogonal polynomial bases with $\Phi_0 := 1$, and $\hat{\mathbf{F}}_i \in \mathbb{R}^{p \times p}$, $\hat{\mathbf{G}}_i \in \mathbb{R}^{p \times q}$, and $\hat{\mathbf{H}}_i \in \mathbb{R}^{r \times p}$, for $i \in \{0, 1, \dots, L-1\}$, are PCE coefficients which can be

calculated using off-the-shelf tools [35]. The approximation precision is guaranteed in a Hilbert sense [36]. Similar expansion can also be performed to \bar{z}_k and \bar{w}_k , with $\bar{z}_k = \sum_{i=0}^{L-1} \hat{z}_{k,i} \Phi_i$, and $\bar{w}_k = \sum_{i=0}^{L-1} \hat{w}_{k,i} \Phi_i$, for $k \in \mathcal{N}$, where $\hat{z}_{k,i} \in \mathbb{R}^p$ and $\hat{w}_{k,i} \in \mathbb{R}^r$ are expansion coefficients of \bar{z}_k and \bar{w}_k , respectively. Applying the above expansions to Eq. (6), we have the following PCE-based dynamic model,

$$\text{OVs (PCE model)} : \begin{cases} \hat{z}_{k+1} = \hat{\mathbf{F}} \hat{z}_k + \hat{\mathbf{G}} \tau_k, \\ \hat{w}_k = \hat{\mathbf{H}} \hat{z}_k, \end{cases} \quad (11)$$

where $\hat{z}_k = [\hat{z}_{k,0}^\top \cdots \hat{z}_{k,L-1}^\top]^\top$ and $\hat{w}_k = [\hat{w}_{k,0}^\top \cdots \hat{w}_{k,L-1}^\top]^\top$ are PCE coefficients, $\hat{\mathbf{F}}$ has $\sum_{i=0}^{L-1} \hat{\mathbf{F}}_i \Psi_{ijr}$ as its j, r -th partition, where $\Psi_{ijr} = E(\Phi_i \Phi_j \Phi_r) / E(\Phi_i^2)$, $j, r \in \{0, 1, \dots, L-1\}$, $\hat{\mathbf{G}} = [\hat{\mathbf{G}}_0^\top \hat{\mathbf{G}}_1^\top \cdots \hat{\mathbf{G}}_{L-1}^\top]^\top$, and $\hat{\mathbf{H}} = \text{diag}(\hat{\mathbf{H}}_0 \hat{\mathbf{H}}_1 \cdots \hat{\mathbf{H}}_{L-1})$. The PCE-based model in Eq. (11) is a generic form of the PCE-based vehicle model in Appx.-C.

Note that a deterministic PCE-based model as Eq. (11) only exists for systems with *epistemic* uncertainty, where η has a time-invariant joint distribution p_η . Utilizing this model, one can precisely quantify the statistics of \bar{z}_k and \bar{w}_k at any time $k \in \mathbb{N}$. For example, the expected value $\mu_{\bar{w}_k}$ and the covariance $\Sigma_{\bar{w}_k}$ of \bar{w}_k read

$$\mu_{\bar{w}_k} = \hat{w}_{k,0}, \quad \Sigma_{\bar{w}_k} = \sum_{i=1}^{L-1} \hat{w}_{k,i} \hat{w}_{k,i}^\top E(\Phi_i^2). \quad (12)$$

This renders the following PCE-facilitated solution which can be solved using off-the-shelf tools such as MIP [26].

PCE-Facilitated Control Solution: For any time $k \in \mathcal{N}$ with historical measurements $y_0 y_1 \cdots y_k \in \mathbf{Y}^+$, solve the following deterministic optimization problem,

$$\min_{\bar{\mathbf{u}}_k} \sum_{i=0}^{N-k-1} \bar{\mathbf{u}}_{i|k}^\top R \bar{\mathbf{u}}_{i|k} \quad (13a)$$

$$\text{s.t. } \tilde{x}_{i+1|k} = A \tilde{x}_{i|k} + B \bar{\mathbf{u}}_{i|k}, \quad (13b)$$

$$\bar{\mathbf{u}}_{i|k} \in \mathbf{U}, \quad \forall i \in \{0, 1, \dots, N-k-1\} \quad (13c)$$

$$\tilde{y}_{i+k|k} = C \tilde{x}_{i|k}, \quad \forall i \in \{0, 1, \dots, N-k\}, \quad (13d)$$

$$\tilde{y}_{r|k} = y_r, \quad \forall r \in \{0, 1, \dots, k\}, \quad (13e)$$

$$\hat{z}_{i+1} = \hat{\mathbf{F}} \hat{z}_i + \hat{\mathbf{G}} \tau_i, \quad \forall i \in \mathcal{H}, \quad (13f)$$

$$\hat{w}_i = \hat{\mathbf{H}} \hat{z}_i, \quad \forall i \in \mathcal{H} \cup \{N\}, \quad (13g)$$

$$\omega_k \models \psi, \quad (13h)$$

where $\omega_k := \omega_{0|k} \omega_{1|k} \cdots \omega_{N|k}$ is a deterministic signal with $\omega_{i|k} := [\tilde{y}_{i|k}^\top \hat{w}_i^\top]^\top$, for $i \in \mathcal{H} \cup \{N\}$ and ψ is an STL formula (see Appx.-A) ensuring $\omega_k \models \psi \rightarrow (\tilde{y}_k, \mathbf{w}) \models \varphi$, which can be straightforwardly determined by substituting the approximation in Eq. (12) to each belief-space predicate of the DSTL formula φ .

Remark 2 (Computational Complexity): The computational complexity of Eq. (13) for each time $k \in \mathcal{H} \cup \{N\}$ is in general exponential to the number of binary variables brought up by the specification constraint Eq. (13h), according to [26]. Since all history output variables $\tilde{y}_{r|k}$ for $r \in \{0, 1, \dots, k\}$ are constrained by equality Eq. (13e) without binary variables, the number of binary variables can be estimated by $O(n(N-k))$, where n is

the maximal number of STL predicates specified for a specific time from k to N . In other words, n depends on the complexity of the task. In this sense, the total computational complexity of problem Eq. (13) at time $k \in \mathcal{H} \cup \{N\}$ is estimated as $O(2^{n(N-k)})$.

Computational complexity has been a common and open problem for formal control methods. To solve this problem, methods of specification decomposition [37] and timing split [21] have been proposed to reduce the task complexity (quantified by n in Remark 2) and horizon (N in Remark 2), respectively. Given these methods, resolving computational complexity for intention-aware control is beyond the scope of this work and will be studied in future work.

V. EXPERIMENTAL STUDIES

This section uses two autonomous driving cases to show the efficacy of our intention-aware control method. The code can be found at <https://zenodo.org/records/11274822>. All experiments are programmed in Python, solved using the *stlpy* [26] and the *chaospy* [38] toolboxes, and run on a ThinkPad Laptop with an Intel® Core i7-10750H CPU. A video demonstration of the experimental studies is available at https://youtu.be/Pvaj_e2hlY0.

A. Case I: Overtaking

We use an overtaking case to show that an intention-aware controller allows an agent to automatically adjust its behavior according to the intents of its opponents. As shown in Fig. 3, an EV needs to overtake an OV without collisions. The EV and the OV are described as deterministic and stochastic linearized bicycle models (see Appx.-B and -C), respectively. The OV has a random length l and a random control offset δ (see Appx.-C), both sampled from non-Gaussian distributions, with l from a uniform distribution $\mathcal{U}(3.99, 4.01)$ and δ from a truncated Gaussian distribution $\mathcal{N}(0, 0.1^2)_{[-0.1, 0.1]}$. We consider three different scenarios where the OV intends to *slow down*, *speed up*, or *switch to the fast lane*, corresponding to *cooperative*, *antagonistic*, and *ignorant* driving styles, respectively.

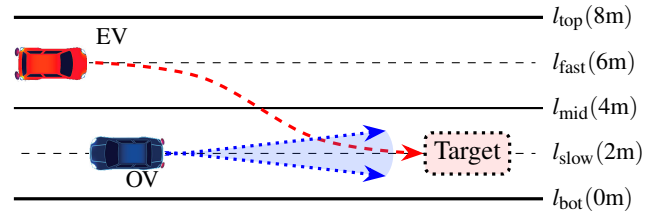


Fig. 3: The overtaking case, where an EV in the fast lane should switch to the slow lane and overtake an OV within a finite time (the dashed arrow). The area in front of the OV bounded by two dotted arrows denotes the joint epistemic uncertainty at a certain risk level.

The overtaking task is first described as natural language. *The EV eventually switches to the slow lane and drives in front of the OV at a maximal risk level 0.05 (95% success*

probability), if the OV does not switch to the fast lane or exceed a speed limit $v_{\text{lim}} = 12\text{m/s}$ (in an average sense). Meanwhile, the EV should always drive inside the lanes and keep a minimal distance with the OV, $d_{\text{safe},1} = 4\text{m}$ longitudinally and $d_{\text{safe},2} = 2\text{m}$ latitudinally, at a maximal risk level 0.05 (95% safe). Then, the task is specified using a DSTL formula for the stochastic model of the OV and converted to an STL formula for its PCE model (See Appx.-D). We solve the MPC problem in Eq. (13) with a discrete-time $\Delta t = 1\text{s}$ and a finite control horizon with length $N = 15$. The control cost is set as $R = \text{diag}(10^4, 10^{-6})$ to penalize over-steering and encourage speed adjustment. Each time we solve Eq. (13), we update the linearized vehicle models using their current states to reduce the impact of linearization errors.

The resulting trajectories of the EV and the OV with various intentions are shown in Fig. 4. We can see that the EV changes its behaviors when the intention of the OV varies. As shown in Fig. 4a), when the OV intends to keep a constant speed and is not expected to exceed the speed limit v_{lim} , the EV performs a successful overtake. When the OV intends to speed up as to exceed the speed limit v_{lim} , as shown in Fig. 4b), the EV decides to give up overtaking and maintains its current speed. When the OV intends to perform an antagonistic lane-switching, as shown in Fig. 4c), the EV slows down and remains in the fast lane to avoid potential collisions. A 100-time Monte Carlo sampling study results in zero collision cases, indicating a risk level lower than 0.05. Thus, the behavior of the EV satisfies the overtaking task specification for all three scenarios despite the linearization errors, implying the efficacy of the proposed intention-aware control method.

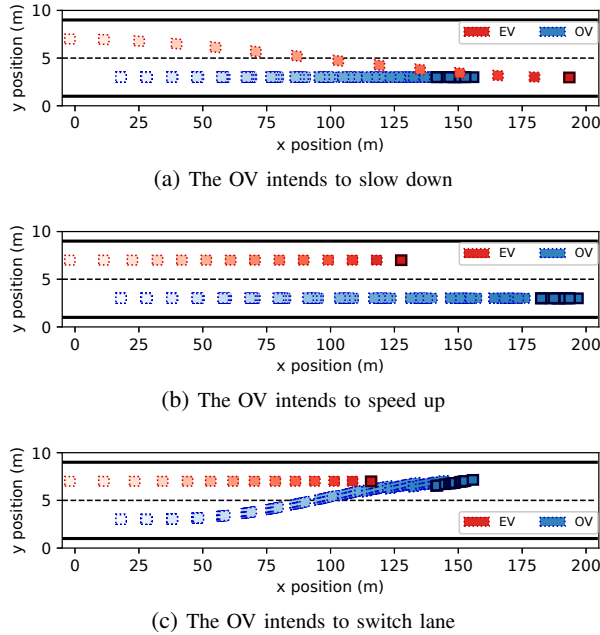


Fig. 4: The vehicle trajectories from a 100-time Monte Carlo study.

The computation time per step for all three scenarios is presented in Fig. 5, showing a clear exponentially decaying

trend which is consistent with our analysis in Remark 2. The *slow down* (for OV) scenario involves heavier computations than the other two since it is the only one that leads to successful EV overtaking. Overall, the overtaking task is sufficiently simple such that all computations have been accomplished within 0.2s, much smaller than the discrete sampling time 1s. This indicates that our method is promising to be deployed to practical vehicles with real-time performance requirements.

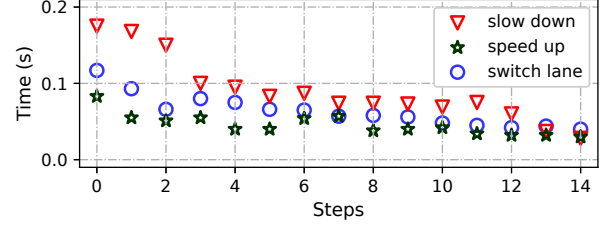


Fig. 5: The computation time per step (Case I).

In each scenario of this case study, we assume that the OV has a certain and unchanged intention known to the EV, which is not always practical in reality. In practice, the EV usually need to infer the OV's intention from its history behavior [39]. Moreover, practical vehicles may reveal different intentions in sequence. In such cases, the EV should not only infer the sequential intentions of the OV but also estimate the time horizons of these intentions. This renders an interesting but challenging sequential intention-aware control problem which is expected to be investigated in future work.

B. Case II: Intersection

In this study, we use the intersection case raised in Sec. I (See Fig. 1) to show how an intention-aware controller ensures risk restriction for uncertain intentions. Similar to Sec. V-A, the EV is described using a deterministic linearized bicycle model while the OV as a stochastic model with an unknown length and a random control offset sampled from a uniform distribution $\mathcal{U}(3.59, 3.61)$ and a Gaussian distribution $\mathcal{N}(0, 0.01^2)$, respectively. Also, we use a similar stochastic vehicle model, with an unknown length sampled from $\mathcal{U}(0.490, 0.501)$ and a random control offset sampled from $\mathcal{N}(0, 0.01^2)$, to denote the distributional behavior of a group of pedestrians. We consider an uncertain intention of the OV with possible intents $\{\text{speed up}, \text{constant speed}, \text{slow down}\}$, corresponding to *antagonistic*, *ignorant*, and *cooperative* driving strategies, respectively. This intention is subject to a uniform distribution $\{1/3, 1/3, 1/3\}$. Also, we assume that the pedestrians have an uncertain intention with intents $\{\text{move fast}, \text{move slowly}\}$ subject to a uniform distribution $\{1/2, 1/2\}$. See Appx.-E for the detailed experimental configurations.

The turning task is first described as natural language. *The EV eventually reaches the target lane. Besides, the EV should only turn beyond the first pedestrian crossing and should always avoid collisions with the OV and the pedestrians at a risk level 0.05.* Then, the task is specified

using a DSTL formula and converted to an STL formula (See Appx.-E) to facilitate a deterministic MPC problem as in Eq. (13). We consider a discrete-time $\Delta t = 0.5$ s, a finite horizon $N = 36$, and a control cost $R = \text{diag}(1, 50)$. Similar to Case I, we update the linearized vehicle models using the most recent measurements before solving the optimization problem Eq. (13) at each time $k \in \{0, 1, \dots, N-1\}$ to mitigate the influence of linearization errors.

We use a comparison study to address the advantage of intention-aware control in risk restriction, where we consider two specifications that omit and incorporate the uncertain intentions of the OV and the pedestrians, respectively (See Appx.-E for details). The resulting trajectories of the vehicles and the pedestrians are shown in Fig. 6. The trajectories of the OV and the pedestrian are the results of 100 times Monte Carlo sampling. The multi-modal distribution of the OV is displayed, with each modal denoting the distribution of a *speeding-up*, a *constant-speed*, and a *slowing-down* intent, respectively. We can see that the *no-awareness* EV is at risk of colliding with the OV for the *speeding-up* intent at time step $k = 16$. The multi-modal characteristics of the pedestrian are not obvious due to its low speed. But we can still see that *no-awareness* EV is at risk of colliding with the *moving-fast* pedestrians at time step $k = 20$. However, the intention-aware EV has successfully avoided collisions with all possible positions of the OV and the pedestrians by turning slightly earlier compared to the *no-awareness* case (See Fig. 6). Although this strategy seems antagonistic and aggressive from a practical perspective, it restricts the risk under the predefined level of 0.05. The results indicate that the developed intention-aware control method ensures restricted risk despite the complex joint uncertainties and linearization errors.

The computation time per step for both *no-awareness* and *intention-awareness* scenarios is presented in Fig. 7. Both scenarios show exponentially decaying computation time as the step increases, implying the correctness of our analysis on computational complexity in Remark 2. It is noticed that the intention-aware controller involves heavier computation than the *no-awareness* one due to the incorporation of uncertain intentions. The computation is substantial before step 10 when the EV tries to find a feasible solution to avoid collisions with the OV and the pedestrians. The computation time before step 8 even exceeds the discrete sampling time 0.5 s, bringing up a challenge to its deployment on a real-time system. Possible solutions to resolve this problem may include the decomposition [37], splitting [21], and conflict resolution [40] of STL specifications for a simplified task, which is beyond the scope of this paper.

VI. DISCUSSION

The most important result of this paper is a tractable and efficient PCE-facilitated solution for the intention-aware control of an autonomous vehicle with uncertain opponent traffic participants. To derive this solution, we describe the opponent participants as stochastic dynamic models with

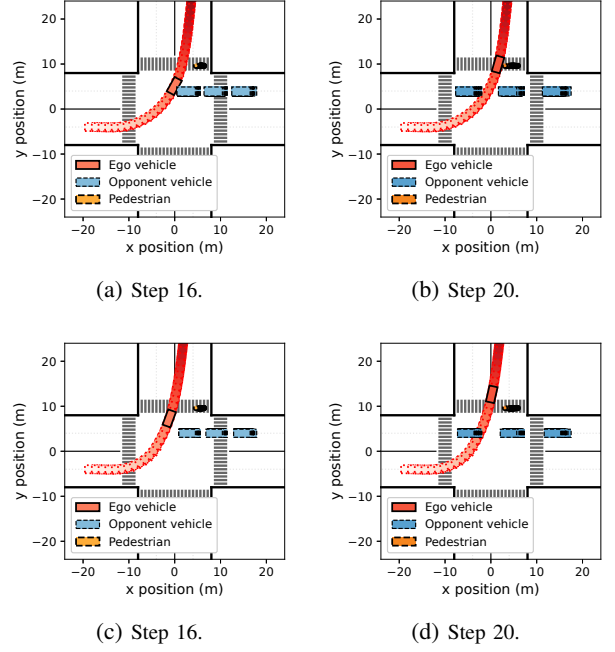


Fig. 6: Results of comparison study. (a) and (b): no awareness, the EV collides with the OV or with the pedestrians; (c) and (d): with intention awareness, no collisions occur.

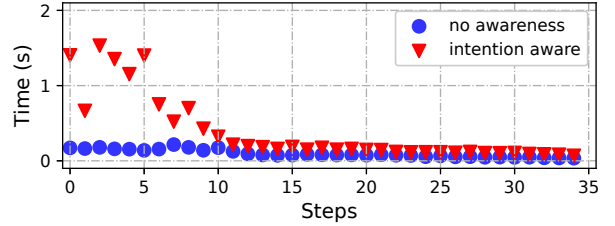


Fig. 7: The computation time per step (Case II).

epistemically uncertain intentions and parameters. This allows us to characterize the random behaviors of these opponents into a deterministic PCE-based model. Through a novel DSTL belief-space specification, we convert a challenging intention-aware control problem into a deterministic MPC problem that can be easily solved using off-the-shelf tools. Besides, the controller is correct-by-design, meaning that it ensures provable risk restriction. Theoretical analysis and experimental studies have implied its promising real-time implementation. Finally, the experimental results have sketched an interactive control strategy that guarantees superior safety and flexibility in complex driving environments compared to the conventional no-awareness controllers.

Our work also has several limitations that are worth studying in future work. Firstly, our method assumes known uncertainty characteristics for all opponents. In practice, however, the intention of an opponent may change and may even be unknown to the ego vehicle. In this case, the characteristics of its intention should be learned and updated using its historical observations. Secondly, the driving tasks have

been specified on a belief space which does not incorporate the historical observations of the opponents. As an extension of this work, it would be interesting to study the restriction of risk incorporating the historical behaviors of the opponents. Thirdly, the computational complexity of the solution could be further reduced using specification separate and split methods.

VII. CONCLUSIONS

This paper provides the first correct-by-design intention-, interaction-, and risk-aware controller for autonomous vehicles by characterizing complex epistemic uncertainty using stochastic expansion. It renders an efficient solution that can be solved using off-the-shelf tools. In the future, we will study the extension of this work to risk-restriction control incorporating observations of the opponents. We will also investigate the reduction of computational complexity of the method.

APPENDIX

A. Signal Temporal Logic (STL)

For a discrete-time signal $\mathbf{s} := s_0 s_1 \dots$, where $s_k \in \mathbb{R}^n$ for $k \in \mathbb{N}$ and $n \in \mathbb{Z}^+$, the syntax of STL is given as [41]

$$\psi ::= \top \mid \mu \mid \neg \psi \mid \psi_1 \wedge \psi_2 \mid \psi_1 \cup_{[a,b]} \psi_2,$$

where ψ_1 , ψ_2 , and μ are STL formulas, μ is a predicate with a mapping $h: \mathbb{R}^n \rightarrow \mathbb{R}$ via $\mu := \begin{cases} \top, & h(s_k) \geq 0 \\ \perp, & h(s_k) < 0 \end{cases}$, $k \in \mathbb{N}$. The *disjunction*, *eventually*, and *always* operators are defined as $\psi_1 \vee \psi_2 := \neg(\neg \psi_1 \wedge \neg \psi_2)$, $F_{[a,b]} \psi := \top \cup_{[a,b]} \psi$, $G_{[a,b]} \psi := \neg(\neg \top \cup_{[a,b]} \neg \psi)$. The semantics of STL denoted as $(\mathbf{s}, k) \models \psi$ are recursively determined as

$$\begin{aligned} (\mathbf{s}, k) &\models \mu \leftrightarrow h(s_k) \geq 0, \quad (\mathbf{s}, k) \models \neg \psi \leftrightarrow \neg((\mathbf{s}, k) \models \psi), \\ (\mathbf{s}, k) &\models \psi_1 \wedge \psi_2 \leftrightarrow (\mathbf{s}, k) \models \psi_1 \wedge (\mathbf{s}, k) \models \psi_2, \\ (\mathbf{s}, k) &\models \psi_1 \vee \psi_2 \leftrightarrow (\mathbf{s}, k) \models \psi_1 \vee (\mathbf{s}, k) \models \psi_2, \\ (\mathbf{s}, k) &\models F_{[a,b]} \psi \leftrightarrow \exists k' \in [k+a, k+b], \text{ s.t., } (\mathbf{s}, k') \models \psi, \\ (\mathbf{s}, k) &\models G_{[a,b]} \psi \leftrightarrow \forall k' \in [k+a, k+b], \text{ s.t., } (\mathbf{s}, k') \models \psi, \\ (\mathbf{s}, k) &\models \psi_1 \cup_{[a,b]} \psi_2 \leftrightarrow \exists k' \in [k+a, k+b], \text{ s.t., } (\mathbf{s}, k') \models \psi_2, \\ &\quad \text{and } \forall k'' \in [k, k'], (\mathbf{s}, k'') \models \psi_1. \end{aligned}$$

For $k = 0$, the symbol k can be omitted, rendering $\mathbf{s} \models \psi$. The robustness of an STL formula ψ denoted as $\rho^\psi(\mathbf{s}, k)$, with $\rho^\psi(\mathbf{s}, k) > 0 \leftrightarrow (\mathbf{s}, k) \models \psi$, is inductively defined as

$$\begin{aligned} \rho^\mu(\mathbf{s}, k) &:= h(s_k), \quad \rho^{\neg \psi}(\mathbf{s}, k) := -\rho^\psi(\mathbf{s}, k), \\ \rho^{\psi_1 \wedge \psi_2}(\mathbf{s}, k) &:= \min(\rho^{\psi_1}(\mathbf{s}, k), \rho^{\psi_2}(\mathbf{s}, k)), \\ \rho^{\psi_1 \vee \psi_2}(\mathbf{s}, k) &:= \max(\rho^{\psi_1}(\mathbf{s}, k), \rho^{\psi_2}(\mathbf{s}, k)), \\ \rho^{\psi_1 \cup_{[a,b]} \psi_2}(\mathbf{s}, k) &:= \max_{k' \in [k+a, k+b]} (\min(\rho^{\psi_2}(\mathbf{s}, k'), \\ &\quad \min_{k'' \in [k, k']} \rho^{\psi_1}(\mathbf{s}, k''))), \\ \rho^{F_{[a,b]} \psi}(\mathbf{s}, k) &:= \max_{k' \in [k+a, k+b]} \rho^\psi(\mathbf{s}, k'), \\ \rho^{G_{[a,b]} \psi}(\mathbf{s}, k) &:= \min_{k' \in [k+a, k+b]} \rho^\psi(\mathbf{s}, k'). \end{aligned}$$

For $k = 0$, the robustness reads $\rho^\psi(\mathbf{s})$.

B. Describing EV Using a Deterministic Linear Model

An autonomous vehicle is typically described as a nonlinear bicycle model [30]. We use a deterministic bicycle model illustrated in Fig. 8 to describe the behavior of the EV,

$$\text{EV} : \begin{cases} \xi_{k+1} = \xi_k + \Delta t \omega_k \cos(\phi_k + \gamma_k), \\ \zeta_{k+1} = \zeta_k + \Delta t \omega_k \sin(\phi_k + \gamma_k), \\ \phi_{k+1} = \phi_k + \Delta t \omega_k \sin \gamma_k / l, \\ \omega_{k+1} = \omega_k + \Delta t a_k, \end{cases} \quad (14)$$

where (ξ_k, ζ_k) denote the planar coordinate of the mass center of the front wheel at discrete time $k \in \mathbb{N}$, ϕ_k and ω_k are the heading angle of the vehicle and the linear velocity of the front wheel, respectively, γ_k , a_k are the steering angle and the linear acceleration of the front wheel, respectively, Δt is the discrete sampling time, and l is the length of the vehicle. Different from [30], all variables in Eq. (14) are defined for the front wheel instead of the mass center of the vehicle to obtain a simplified model. In fact, it is straightforward to convert Eq. (14) to a model for an arbitrary point on the vehicle. Let (ξ_k^a, ζ_k^a) , ϕ_k^a , and ω_k^a be the planar coordinate, the heading angle, and the linear velocity of any mass point on the vehicle as shown in Fig. 8, their relations with the front wheel variables (ξ_k, ζ_k) , ϕ_k , and ω_k are described by $\xi_k^a = \xi_k - (1-c)l \cos \phi_k$, $\zeta_k^a = \zeta_k - (1-c)l \sin \phi_k$, $\omega_k^a = \omega_k \cos \gamma_k / \cos \gamma_k^a$, and $\gamma_k^a = \tan^{-1}(c \tan \gamma_k)$, where $c \in [0, 1]$ is a ratio scalar such that cl is the distance from this point to the back wheel.

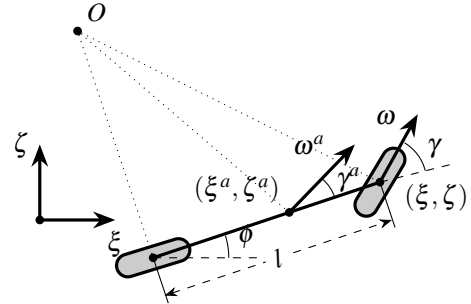


Fig. 8: The bicycle model for autonomous vehicles.

Let $x_k = [\xi_k \ \zeta_k \ \phi_k \ \omega_k]^\top$ be the measurable state of EV and $u_k = [\gamma_k \ a_k]^\top$ be its control input. The deterministic model of the EV is compactly represented as

$$\text{EV} : \begin{cases} x_{k+1} = x_k + f(x_k, u_k), \\ y_k = x_k, \end{cases} \quad (15)$$

where $y_k \in \mathbb{R}^4$ is the output of EV and

$$f(x_k, u_k) = \Delta t \begin{bmatrix} \omega_k \cos(\phi_k + \gamma_k) & \omega_k \sin(\phi_k + \gamma_k) & \frac{\omega_k \sin \gamma_k}{l} & a_k \end{bmatrix}^\top.$$

By linearizing Eq. (15) around $x_0 = [\xi_0 \ \zeta_0 \ \phi_0 \ \omega_0]^\top$ and $u_0 = [\gamma_0 \ a_0]^\top$, we obtain a linearized dynamic model,

$$f(x_k, u_k) = f(x_0, u_0) + A(x_0, u_0)(x_k - x_0) + B(x_0, u_0)(u_k - u_0),$$

where $A(x_0, u_0) \in \mathbb{R}^{4 \times 4}$ and $B(x_0, u_0) \in \mathbb{R}^{4 \times 2}$ are

$$A(x_0, u_0) = \begin{bmatrix} 0 & 0 & -\Delta t \omega_0 \sin(\phi_0 + \gamma_0) & \Delta t \cos(\phi_0 + \gamma_0) \\ 0 & 0 & \Delta t \omega_0 \cos(\phi_0 + \gamma_0) & \Delta t \sin(\phi_0 + \gamma_0) \\ 0 & 0 & 0 & \Delta t \sin \gamma_0 / l \\ 0 & 0 & 0 & 0 \end{bmatrix},$$

$$B(x_0, u_0) = \begin{bmatrix} -\Delta t \omega_0 \sin(\phi_0 + \gamma_0) & 0 \\ \Delta t \omega_0 \cos(\phi_0 + \gamma_0) & 0 \\ \Delta t \omega_0 \cos \gamma_0 / l & 0 \\ 0 & \Delta t \end{bmatrix}.$$

Assume $\phi_k \approx \phi_0$ for all $k \in \mathbb{N}$ since a vehicle hardly performs large steering. With $\gamma_0 = 0$, we rewrite (15) as

$$\text{EV} : \begin{cases} x_{k+1} = A_0 x_k + B_0 u_k + d_0, \\ y_k = C_0 x_k, \end{cases} \quad (16)$$

which is consistent with the EV model in Eq. (1), where $y_k \in \mathbb{R}^4$ is the output of EV, $C_0 = I$, and

$$A_0 = I + \Delta t \begin{bmatrix} 0 & 0 & -\omega_0 \sin \phi_0 & \cos \phi_0 \\ 0 & 0 & \omega_0 \cos \phi_0 & \sin \phi_0 \\ 0 & 0 & 0 & 0 \\ 0 & 0 & 0 & 0 \end{bmatrix},$$

$$B_0 = \Delta t \begin{bmatrix} -\omega_0 \sin \phi_0 & 0 \\ \omega_0 \cos \phi_0 & 0 \\ 0 & 0 \\ 0 & 1 \end{bmatrix}, d_0 = \Delta t \begin{bmatrix} \omega_0 \phi_0 \sin \phi_0 \\ -\omega_0 \phi_0 \cos \phi_0 \\ 0 \\ 0 \end{bmatrix}.$$

C. Describing OV Using a Stochastic Linear Model

Based on Eq. (14), we use a stochastic bicycle model to describe the behavior of an OV with uncertain parameters,

$$\text{OV} : \begin{cases} \xi_{k+1} = \xi_k + \Delta t \omega_k \cos(\phi_k + \gamma_k), \\ \zeta_{k+1} = \zeta_k + \Delta t \omega_k \sin(\phi_k + \gamma_k), \\ \phi_{k+1} = \phi_k + \Delta t \omega_k \sin \gamma_k / l, \\ \omega_{k+1} = \omega_k + \Delta t (a_k + \delta), \end{cases} \quad (17)$$

where $l \sim p_l$ is the unknown length of the vehicle and $\delta \sim p_\delta$ is a random acceleration control offset, where p_l and p_δ are predefined PDFs. We assume an integer-valued intention variable $\iota \in I \subset \mathbb{Z}$ with a distribution p_ι on I and an intention-encoding feedforward controller $v_k = \iota \tau_k$ for the OV, where $v_k = [\gamma_k, a_k]^\top$ is the control input of the OV and $\tau_k \in \mathbb{R}^2$ for $k \in \mathbb{N}$ is a predefined control signal. Supposing that the feedforward control input τ_0, τ_1, \dots is designed such that $v_k = \tau_k$ leads to an accelerating OV, the intents $\iota = -1, 0, 1$ encode the *slowing-down*, *constant-speed*, and *speeding-up* driving policies, respectively.

Let $z_k = [\xi_k \ \zeta_k \ \phi_k \ \omega_k]^\top$ be the measurable state of the OV. Similar to Appx.-B, we obtain the following linearized dynamic model around $z_0 = [\xi_0 \ \zeta_0 \ \phi_0 \ \omega_0]^\top$,

$$\text{OV} : \begin{cases} z_{k+1} = A_0 z_k + \sum_{i=0}^1 b_i(\eta) B_i \tau_k + \sum_{i=0}^1 e_i(\eta) d_i, \\ w_k = C_0 z_k, \end{cases} \quad (18)$$

where $\eta = [l \ \delta \ \iota]^\top$ is a joint random variable, $b_0(\eta) = \iota$, $b_1(\eta) = \iota/l$, $e_0(\eta) = 1$, and $e_1(\eta) = \delta$, A_0 , B_0 , C_0 , and d_0 are defined in Eq. (16), and

$$B_1 = \Delta t \begin{bmatrix} 0 & 0 \\ 0 & 0 \\ \omega_0 \cos \phi_0 & 0 \\ 0 & 0 \end{bmatrix} \text{ and } d_1 = \Delta t \begin{bmatrix} 0 \\ 0 \\ 0 \\ 1 \end{bmatrix}. \quad (19)$$

The stochastic model Eq. (18) has a consistent form with the OV model in Eq. (6).

We use PCE to expand the state and uncertain parameters of Eq. (18) as $z_k = \sum_{j=0}^{L-1} \hat{z}_{k,j} \Phi_j$ for $k \in \mathbb{N}$, $b_0(\eta) = \hat{\mathbf{b}}_0^\top \Phi$, $b_1(\eta) = \hat{\mathbf{b}}_1^\top \Phi$, $e_0(\eta) = \hat{\mathbf{e}}_0^\top \Phi$, $e_1(\eta) = \hat{\mathbf{e}}_1^\top \Phi$, where $\Phi = [\Phi_0, \Phi_1, \dots, \Phi_{L-1}]^\top$ is the polynomial bases of the joint uncertainty η with $\Phi_0 := 1$, $\hat{z}_{k,j} \in \mathbb{R}^4$ for $j = 0, 1, \dots, L-1$ and $\hat{\mathbf{b}}_0, \hat{\mathbf{b}}_1, \hat{\mathbf{e}}_0, \hat{\mathbf{e}}_1 \in \mathbb{R}^L$ are vectors of PCE coefficients. Substituting the expansions above to Eq. (18) renders

$$\sum_{j=0}^{L-1} \hat{z}_{k+1,j} \Phi_j = A_0 \sum_{j=0}^{L-1} \hat{z}_{k,j} \Phi_j + \sum_{i=0}^1 \hat{\mathbf{b}}_i^\top \Phi B_i \tau_k + \sum_{i=0}^1 \hat{\mathbf{e}}_i^\top \Phi d_i.$$

Taking the inner product of both sides with any polynomial bases Φ_s , $s \in \{0, 1, \dots, L-1\}$, we have

$$\sum_{j=0}^{L-1} \hat{z}_{k+1,j} \langle \Phi_j, \Phi_s \rangle = \sum_{j=0}^{L-1} A_0 \hat{z}_{k,j} \langle \Phi_j, \Phi_s \rangle + \sum_{i=0}^1 \hat{\mathbf{b}}_i^\top \langle \Phi, \Phi_s \rangle B_i \tau_k + \sum_{i=0}^1 \hat{\mathbf{e}}_i^\top \langle \Phi, \Phi_s \rangle d_i.$$

The orthogonal properties of the bases ensure $\langle \Phi_s, \Phi_s \rangle > 0$, $\forall s \in \{0, 1, \dots, N-1\}$ and $\langle \Phi_j, \Phi_s \rangle = 0$, $\forall j, s \in \{0, 1, \dots, L-1\}$, $j \neq s$. The PCE model of the OV reads

$$\hat{\mathbf{z}}_{k+1} = \mathbf{A} \hat{\mathbf{z}}_k + \mathbf{B} \tau_k + \mathbf{d}, \quad \hat{\mathbf{w}}_k = \hat{\mathbf{z}}_k, \quad (20)$$

where $\hat{\mathbf{z}}_k = [\hat{z}_{k,0}^\top \ \hat{z}_{k,1}^\top \ \dots \ \hat{z}_{k,L-1}^\top]^\top$, $\mathbf{A} = \text{diag}(\underbrace{A_0, \dots, A_0}_L)$,

$$\mathbf{B} = \begin{bmatrix} \sum_{i=0}^1 \hat{b}_{i,0} B_i \\ \sum_{i=0}^1 \hat{b}_{i,1} B_i \\ \vdots \\ \sum_{i=0}^1 \hat{b}_{i,L-1} B_i \end{bmatrix}, \text{ and } \mathbf{d} = \begin{bmatrix} \sum_{i=0}^1 \hat{e}_{i,0} d_i \\ \sum_{i=0}^1 \hat{e}_{i,1} d_i \\ \vdots \\ \sum_{i=0}^1 \hat{e}_{i,L-1} d_i \end{bmatrix}.$$

with an initial condition $\hat{\mathbf{z}}_0 = [z_0^\top \ \underbrace{\mathbf{0}_{4 \times 1}^\top \ \dots \ \mathbf{0}_{4 \times 1}^\top}_{L-1}]^\top$, where

$\hat{b}_{i,j}$ and $\hat{e}_{i,j}$ are the j -th element of vectors $\hat{\mathbf{b}}_i$ and $\hat{\mathbf{e}}_i$, for $i \in \{0, 1\}$ and $j \in \{0, 1, \dots, L-1\}$. Eq. (20) is consistent with the PCE-based model of the OVs in Eq. (11).

D. Experimental Configuration of Case I

Case I considers a deterministic EV modeled by Eq. (1) and a stochastic OV modeled by Eq. (3). The details of the models are given Appx.-B and Appx.-C. We use a deterministic variable $y_k \in \mathbb{R}^4$ and a stochastic variable $w_k \in \mathbb{R}^4$ to represent the outputs of the EV and OV, respectively. The elements of these variables, i.e., $y_{i,k}$ and $w_{i,k}$ for $i \in \{1, 2, 3, 4\}$, denote the longitudinal positions, the latitudinal positions, the orientations, and the linear velocities of the vehicles.

Following the natural language description in Sec. V-A, the overtaking task is specified as DSTL predicates: *The EV eventually switches to the slow lane* ($(v_1^E, *) := |y_{2,k} - l_{\text{slow}}| < 0.1m \wedge |y_{3,k}| < 0.1rad$) and *drives in front of the OV at a maximal risk level 0.05* ($(v_2^E, 0.05) := P(w_{1,k} \leq y_{1,k} - d_{\text{safe},1}) \geq 0.95$), *if the OV does not switch to the fast lane* ($(v_1^O, 1) := \mu_{w_{2,k}} < l_{\text{mid}}$) or *exceed a speed limit* ($(v_2^O, 1) := \mu_{w_{4,k}} < v_{\text{lim}}$). Meanwhile, *the EV should always drive inside the lanes* ($(v_1^S, *) := l_{\text{bot}} < y_{2,k} \leq l_{\text{top}}$) and *keep a minimal distance*

with the OV, $d_{\text{safe},1} = 10\text{m}$ longitudinally and $d_{\text{safe},2} = 2\text{m}$ latitudinally, at a maximal risk level 0.05 ($(v_2^S, 0.05) := P(|w_{1,k} - y_{1,k}| < d_{\text{safe},1} \wedge |w_{2,k} - y_{2,k}| < d_{\text{safe},2}) \geq 0.95$). Here, $*$ denotes an arbitrary value in $[0, 1]$. Then, this task is specified as $\varphi := G_{[0,N]} \bigwedge_{j=1}^2 (v_j^S, 0.05) \wedge (G_{[0,N]} \bigwedge_{j=1}^2 (v_j^O, 1) \rightarrow F_{[0,N-3]} G_{[0,3]} \bigwedge_{j=1}^2 (v_j^E, 0.05))$. Using Eq. (12), we convert the DSTL formula φ into an STL formula.

E. Experimental Configuration of Case II

Case II considers a deterministic EV modeled by Eq. (1) and a stochastic OV modeled by Eq. (3). The details of the models are given Appx.-B and Appx.-C. We use a deterministic variable $y_k \in \mathbb{R}^4$ and a stochastic variable $w_k \in \mathbb{R}^4$ to represent the outputs of the EV and OV, respectively. Besides, we use another stochastic OV model to denote the dynamics of a group of pedestrians, with a stochastic output variable $p_k \in \mathbb{R}^4$. The elements of these variables, i.e., $y_{i,k}$, $w_{i,k}$, and $p_{i,k}$ for $i \in \{1, 2, 3, 4\}$ denote the longitudinal positions, the latitudinal positions, the orientations, and the linear velocities of the EV, the OV, and the pedestrian, respectively.

Following the natural language description in Sec. V-B, the turning task is specified as DSTL predicates: *The EV eventually reaches the target lane* ($(v_1^E, *) := |y_{1,k} - l/2| < 0.1\text{m} \wedge y_{2,k} > 3l/2$). *Besides, the EV should only turn after the first pedestrian crossing* ($(v_2^E, *) : (y_{1,k} < -1.2l) \rightarrow (|y_{2,k} + l/2| < 0.1\text{m})$) *and should always avoid collisions with the OV and the pedestrians at a risk level 0.05* ($(v_2^S, 0.05) := P(|w_{1,k} - y_{1,k}| < d_{\text{safe},1}^O \wedge |w_{2,k} - y_{2,k}| < d_{\text{safe},2}^O) \geq 0.95$ and $(v_2^S, 0.05) := P(|p_{1,k} - y_{1,k}| < d_{\text{safe},1}^P \wedge |p_{2,k} - y_{2,k}| < d_{\text{safe},2}^P) \geq 0.95$). Here, $*$ denotes an arbitrary value in $[0, 1]$, $l = 8\text{m}$ is the width of each lane, and $d_{\text{safe},i}^O = 4\text{m}$ and $d_{\text{safe},i}^P = 2\text{m}$ are safe distances between the EV and the OV and the pedestrians, respectively, for $i \in \{1, 2\}$ representing the longitudinal and latitudinal directions, respectively.

The intention-aware DSTL specification for the task is $\varphi := (G_{[0,N]} \bigwedge_{j=1}^2 (v_j^S, 0.05)) \wedge (F_{[0,N-3]} G_{[0,3]} \bigwedge_{j=1}^2 (v_j^E, *))$. The no-intention one is $\varphi' := (F_{[0,N-3]} G_{[0,3]} \bigwedge_{j=1}^2 (v_j^E, *))$. Using Eq. (12), we convert these DSTL formulas into STL formulas for the comparison study.

REFERENCES

- [1] J. S. Park, C. Park, and D. Manocha, "I-planner: Intention-aware motion planning using learning-based human motion prediction," *The International Journal of Robotics Research*, vol. 38, no. 1, pp. 23–39, 2019.
- [2] X. Wu, R. Chandra, T. Guan, A. Bedi, and D. Manocha, "Intent-aware planning in heterogeneous traffic via distributed multi-agent reinforcement learning," in *Conference on Robot Learning*. PMLR, 2023, pp. 446–477.
- [3] B. Varga, D. Yang, and S. Hohmann, "Intention-aware decision-making for mixed intersection scenarios," in *2023 IEEE 17th International Symposium on Applied Computational Intelligence and Informatics (SACI)*. IEEE, 2023, pp. 000 369–000 374.
- [4] H. Bai, S. Cai, N. Ye, D. Hsu, and W. S. Lee, "Intention-aware online POMDP planning for autonomous driving in a crowd," in *2015 IEEE International Conference on Robotics and Automation (ICRA)*. IEEE, 2015, pp. 454–460.
- [5] T. Bandyopadhyay, K. S. Won, E. Frazzoli, D. Hsu, W. S. Lee, and D. Rus, "Intention-aware motion planning," in *Algorithmic Foundations of Robotics X: Proceedings of the Tenth Workshop on the Algorithmic Foundations of Robotics*. Springer, 2013, pp. 475–491.
- [6] S. Qi and S.-C. Zhu, "Intent-aware multi-agent reinforcement learning," in *2018 IEEE International Conference on Robotics and Automation (ICRA)*. IEEE, 2018, pp. 7533–7540.
- [7] W. Zhao, J. P. Queralta, and T. Westerlund, "Sim-to-real transfer in deep reinforcement learning for robotics: A survey," in *2020 IEEE Symposium Series on Computational Intelligence (SSCI)*. IEEE, 2020, pp. 737–744.
- [8] X. Li, Z. Serlin, G. Yang, and C. Belta, "A formal methods approach to interpretable reinforcement learning for robotic planning," *Science Robotics*, vol. 4, no. 37, p. eaay6276, 2019.
- [9] C.-J. Hoel, K. Wolff, and L. Laine, "Ensemble quantile networks: Uncertainty-aware reinforcement learning with applications in autonomous driving," *IEEE Transactions on Intelligent Transportation Systems*, 2023.
- [10] A. Salamaty, S. Soudjani, and M. Zamani, "Data-driven verification of stochastic linear systems with signal temporal logic constraints," *Automatica*, vol. 131, p. 109781, 2021.
- [11] T. Badings, L. Romao, A. Abate, and N. Jansen, "Probabilities are not enough: Formal controller synthesis for stochastic dynamical models with epistemic uncertainty," in *Proceedings of the AAAI Conference on Artificial Intelligence*, vol. 37, no. 12, 2023, pp. 14 701–14 710.
- [12] M. H. W. Engelaar, Z. Zhang, M. Lazar, and S. Haesaert, "Risk-aware MPC for stochastic systems with runtime temporal logics," *arXiv preprint arXiv:2402.03165*, 2024.
- [13] S. S. Farahani, R. Majumdar, V. S. Prabhu, and S. Soudjani, "Shrinking horizon model predictive control with signal temporal logic constraints under stochastic disturbances," *IEEE Transactions on Automatic Control*, vol. 64, no. 8, pp. 3324–3331, 2018.
- [14] S. Haesaert, P. Nilsson, C. I. Vasile, R. Thakker, A.-a. Aghamohammadi, A. D. Ames, and R. M. Murray, "Temporal logic control of POMDPs via label-based stochastic simulation relations," *IFAC-PapersOnLine*, vol. 51, no. 16, pp. 271–276, 2018.
- [15] D. N. Jansen, F. Nielson, and L. Zhang, "Belief bisimulation for hidden Markov models: Logical characterisation and decision algorithm," in *NASA Formal Methods: 4th International Symposium, NFM 2012, Norfolk, VA, USA, April 3-5, 2012. Proceedings 4*. Springer, 2012, pp. 326–340.
- [16] A. Jones, M. Schwager, and C. Belta, "Distribution temporal logic: Combining correctness with quality of estimation," in *52nd IEEE Conference on Decision and Control*. IEEE, 2013, pp. 4719–4724.
- [17] K. Leahy, E. Cristofalo, C.-I. Vasile, A. Jones, E. Montijano, M. Schwager, and C. Belta, "Control in belief space with temporal logic specifications using vision-based localization," *The International Journal of Robotics Research*, vol. 38, no. 6, pp. 702–722, 2019.
- [18] D. Sadigh and A. Kapoor, "Safe control under uncertainty with probabilistic signal temporal logic," in *Proceedings of Robotics: Science and Systems XII*, 2016.
- [19] T. A. N. Heirung, J. A. Paulson, J. O'Leary, and A. Mesbah, "Stochastic model predictive control—how does it work?" *Computers & Chemical Engineering*, vol. 114, pp. 158–170, 2018.
- [20] K. Leahy, A. Jones, and C.-I. Vasile, "Fast decomposition of temporal logic specifications for heterogeneous teams," *IEEE Robotics and Automation Letters*, vol. 7, no. 2, pp. 2297–2304, 2022.
- [21] Z. Zhang and S. Haesaert, "Modularized control synthesis for complex signal temporal logic specifications," in *2023 62nd IEEE Conference on Decision and Control (CDC)*. IEEE, 2023, pp. 7856–7861.
- [22] L. Lindemann, M. Cleaveland, G. Shim, and G. J. Pappas, "Safe planning in dynamic environments using conformal prediction," *IEEE Robotics and Automation Letters*, 2023.
- [23] M. S. Eldred and H. C. Elman, "Design under uncertainty employing stochastic expansion methods," *International Journal for Uncertainty Quantification*, vol. 1, no. 2, 2011.
- [24] L. Dai, Y. Xia, and Y. Gao, "Distributed model predictive control of linear systems with stochastic parametric uncertainties and coupled probabilistic constraints," *SIAM Journal on Control and Optimization*, vol. 53, no. 6, pp. 3411–3431, 2015.
- [25] A. Der Kiureghian and O. Ditlevsen, "Aleatory or epistemic? Does it matter?" *Structural Safety*, vol. 31, no. 2, pp. 105–112, 2009.
- [26] V. Kurtz and H. Lin, "Mixed-integer programming for signal temporal logic with fewer binary variables," *IEEE Control Systems Letters*, vol. 6, pp. 2635–2640, 2022.
- [27] N. Dang, T. Shi, Z. Zhang, W. Jin, M. Leibold, and M. Buss, "Identifying reaction-aware driving styles of stochastic model predictive controlled vehicles by inverse reinforcement learning," in *2023 IEEE*

- 26th International Conference on Intelligent Transportation Systems (ITSC). IEEE, 2023, pp. 2887–2892.
- [28] V. Lefkopoulos, M. Menner, A. Domahidi, and M. N. Zeilinger, “Interaction-aware motion prediction for autonomous driving: A multiple model Kalman filtering scheme,” *IEEE Robotics and Automation Letters*, vol. 6, no. 1, pp. 80–87, 2020.
 - [29] T. Brüdigam, M. Olbrich, D. Wollherr, and M. Leibold, “Stochastic model predictive control with a safety guarantee for automated driving,” *IEEE Transactions on Intelligent Vehicles*, 2021.
 - [30] J. Kong, M. Pfeiffer, G. Schildbach, and F. Borrelli, “Kinematic and dynamic vehicle models for autonomous driving control design,” in *2015 IEEE Intelligent Vehicles Symposium (IV)*. IEEE, 2015, pp. 1094–1099.
 - [31] L. Fagiano and M. Khammash, “Nonlinear stochastic model predictive control via regularized polynomial chaos expansions,” in *2012 IEEE 51st IEEE Conference on Decision and Control (CDC)*. IEEE, 2012, pp. 142–147.
 - [32] H. Ahn, C. Chen, I. M. Mitchell, and M. Kamgarpour, “Safe motion planning against multimodal distributions based on a scenario approach,” *IEEE Control Systems Letters*, vol. 6, pp. 1142–1147, 2021.
 - [33] A. M. McKeand, R. M. Gorguluarlan, and S.-K. Choi, “Stochastic analysis and validation under aleatory and epistemic uncertainties,” *Reliability Engineering & System Safety*, vol. 205, p. 107258, 2021.
 - [34] G. C. Calafiore and L. E. Ghaoui, “On distributionally robust chance-constrained linear programs,” *Journal of Optimization Theory and Applications*, vol. 130, pp. 1–22, 2006.
 - [35] F. Petzke, A. Mesbah, and S. Streif, “Pocet: a polynomial chaos expansion toolbox for matlab,” *IFAC-PapersOnLine*, vol. 53, no. 2, pp. 7256–7261, 2020.
 - [36] T. Crestaux, O. Le Maître, and J.-M. Martinez, “Polynomial chaos expansion for sensitivity analysis,” *Reliability Engineering & System Safety*, vol. 94, no. 7, pp. 1161–1172, 2009.
 - [37] M. Charitidou and D. V. Dimarogonas, “Signal temporal logic task decomposition via convex optimization,” *IEEE Control Systems Letters*, vol. 6, pp. 1238–1243, 2021.
 - [38] J. Feinberg, V. G. Eck, and H. P. Langtangen, “Multivariate polynomial chaos expansions with dependent variables,” *SIAM Journal on Scientific Computing*, vol. 40, no. 1, pp. A199–A223, 2018.
 - [39] Y. Xing, C. Lv, H. Wang, H. Wang, Y. Ai, D. Cao, E. Velenis, and F.-Y. Wang, “Driver lane change intention inference for intelligent vehicles: Framework, survey, and challenges,” *IEEE Transactions on Vehicular Technology*, vol. 68, no. 5, pp. 4377–4390, 2019.
 - [40] T. Yang, Y. Zou, S. Li, and Y. Yang, “Distributed model predictive control for probabilistic signal temporal logic specifications,” *IEEE Transactions on Automation Science and Engineering*, 2023.
 - [41] A. Donzé, “On signal temporal logic,” in *Runtime Verification: 4th International Conference, RV 2013, Rennes, France, September 24–27, 2013. Proceedings 4*. Springer, 2013, pp. 382–383.